Chemical Engineering Science 66 (2011) 6014–6027

Contents lists available at SciVerse ScienceDirect

Chemical Engineering Science

journal homepage: www.elsevier.com/locate/ces

Flow of wet powder in a conical centrifugal filter—an analytical model

A.F.M. Bizard, D.D. Symons *

Cambridge University Engineering Department, Trumpington Street, Cambridge CB2 1PZ, UK

ARTICLE INFO

Article history:
Received 14 March 2011
Received in revised form
12 August 2011
Accepted 14 August 2011
Available online 25 August 2011

Keywords:
Centrifugation
Filtration
Laminar flow
Porous Media
Powder technology
Drying

ABSTRACT

A one-dimensional analytical model is developed for the steady state, axisymmetric, slender flow of saturated powder in a rotating perforated cone. Both the powder and the fluid spin with the cone with negligible slip in the hoop direction. They migrate up the wall of the cone along a generator under centrifugal force, which also forces the fluid out of the cone through the powder layer and the porous wall. The flow thus evolves from an over-saturated paste at inlet into a nearly dry powder at outlet. The powder is treated as a Mohr–Coulomb granular solid of constant void fraction and permeability. The shear traction at the wall is assumed to be velocity and pressure dependent. The fluid is treated as Newtonian viscous. The model provides the position of the *colour line* (the transition from over- to under-saturation) and the flow velocity and thickness profiles over the cone. Surface tension effects are assumed negligible compared to the centrifugal acceleration. Two alternative conditions are considered for the flow structure at inlet: fully settled powder at inlet, and progressive settling of an initially homogeneous slurry. The position of the colour line is found to be similar for these two cases over a wide range of operating conditions. Dominant dimensionless groups are identified which control the position of the colour line in a continuous conical centrifuge. Experimental observations of centrifuges used in the sugar industry provide preliminary validation of the model.

1. Introduction

Centrifugal filters are commonly used in the food processing and chemical industries in order to separate the liquid and solid phases of a mixture, where the two phases have comparable densities. There exist two main types of centrifugal filter: *batch* machines with a cylindrical basket and *continuous* machines with a conical basket. The present study focuses on continuous conical centrifuges, which are most commonly used in the sugar industry to separate sucrose crystals from molasses. Swindells (1982) and Greig (1995) extensively studied these machines in a semi-empirical fashion. While their work provides valuable insight in the operation of conical centrifuges in the sugar industry it does not fully address the underlying mechanics. Consequently, only a limited number of operating parameters can be used to optimize the sugar machine and application of their results to pharmaceutical, chemical or other food products is difficult. This study aims at developing a more general model of the continuous centrifugal filter.

The operation of a continuous centrifuge in the sugar industry is now described. The rotating basket of the machine, sketched in Fig. 1, is conical with a jump in cone angle along its length: a lower impervious cone has a semi-angle of $\alpha = 15^\circ$ whereas the upper perforated cone has $\alpha = 30^\circ$. The basket is about 1 m in diameter at outlet and spins at 1000 RPM to provide a maximum centripetal acceleration of 500*g*. The inside wall of the upper, perforated cone is fitted with a slotted screen, thereby allowing for fluid drainage but preventing crystal losses. Slip of the sugar crystals against the screen is favoured by the use of smooth perforated screens with narrow slots and open areas of only 10–15%. The feedstock, in the form of a sugar/molasses slurry (*massecuite*), of liquid volume fraction 50% and temperature 60 °C, is introduced along the spin axis into the lower impervious cone at a constant flow rate. The slurry acquires the angular velocity of the basket and migrates up the wall of the lower cone into the upper, perforated cone under centrifugal force. In an initial region, labelled region I in Fig. 2, the flow is still over-saturated. Liquid drainage causes the slurry to quickly evolve into a cake of densely packed powder, the top of which is damp while the bottom is still saturated with liquid (region II). Finally, in region III only a residual liquid fraction remains and the flow consists of a cake of damp powder sliding over the screen. Region II is the transition zone between flow of over-saturated powder (region I) and flow of damp powder (region III) and is commonly called the *colour line* in the sugar industry. Further liquid drainage in region III is assumed to be negligible and the damp powder is therefore treated as a homogeneous continuous medium of constant properties.

* Corresponding author. Tel.: +44 1223 760502; fax: +44 1223 332662.
E-mail address: dds11@cam.ac.uk (D.D. Symons).

0009-2509/$ - see front matter © 2011 Elsevier Ltd. All rights reserved.
doi:10.1016/j.ces.2011.08.022

While the microstructure of the flow in regions II and III is clear, in region I it depends largely on the operating conditions as we shall now discuss. In the current study we consider the case where the particles are denser than the fluid, so that they tend to settle onto and slide against the wall instead of floating on top of the fluid. At the start of the upper, perforated cone a fraction of the particles may have already settled onto the wall and the remaining powder may not be homogeneously distributed in the overlying fluid. In this analysis we shall consider two idealized extremes: in a first case all the solid particles are assumed settled and sliding before the flow reaches the inlet of the perforated cone; in a second case the flow is still a homogeneous slurry at inlet, with only minimal initial sedimentation. Although the actual flow condition at inlet is expected to be somewhere between these two extremes, we will show that the difference in position of the colour line resulting from these two cases is small. The microstructure considered in each of the three regions is shown in Fig. 3.

In order to develop an analytical model for the flow in a continuous conical centrifuge we will first present some results from the literature. Based on these results we then develop a one-dimensional model of the flow in a continuous conical centrifuge.

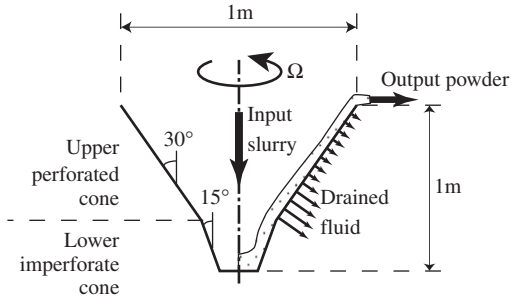

Fig. 1. Section of a typical sugar conical continuous centrifuge.

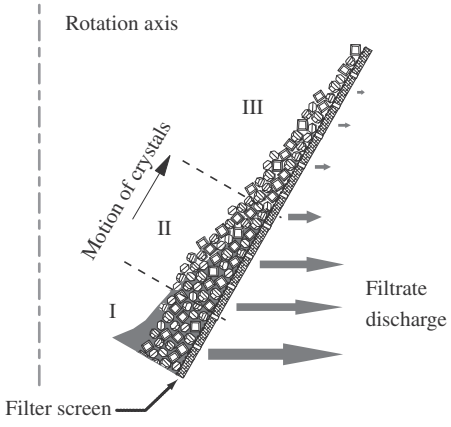

Fig. 2. Flow in a rotating perforated cone.

This model is then non-dimensionalized and solved numerically for a typical application of the conical centrifuge: the separation of liquid molasses from sugar crystals in the sugar industry. Preliminary validation of the model is provided by observation of an industrial centrifuge.

2. Model assumptions

2.1. Slender centrifugal flow

A spherical co-ordinate system (r,θ,ϕ) (see Fig. 4) is appropriate for describing the flow in a conical centrifugal filter. In most practical situations the flow in the cone is slender: its thickness h is significantly smaller than the radial co-ordinate r. A boundary layer approximation of the momentum equations is therefore applicable. This approach to analysis of flow in a spinning cone has been adopted by Bruin (1969) and Makarytchev et al. (1997, 1998) for a Newtonian viscous fluid, and by Symons (2011b) for a damp powder.

The relative importance of convective, Coriolis and centripetal accelerations in the momentum equations (when written in a rotating frame of reference) may be assessed via the Rossby number Ro as defined by (Makarytchev et al., 1997)

$$Ro = \frac{u}{r\Omega \sin\alpha} \approx \frac{\text{convective}}{\text{Coriolis}} \approx \frac{\text{Coriolis}}{\text{centripetal}} \tag{1}$$

where u is the through-thickness averaged radial velocity, Ω the angular velocity of the cone and α is the cone apex angle. In this study we assume that the Rossby number is significantly smaller than unity, so that both convective and Coriolis accelerations are negligible compared to the centripetal acceleration. This assumption is in accordance with observations of typical slender, high viscosity flows observed in industrial conical centrifuges. A consequence of a small Rossby number (i.e. low radial velocity) is that the circumferential slip (in the ϕ-direction) is negligible and therefore the flow has virtually the same angular velocity as the cone at any radius r (see e.g. Symons, in press, 2011b).

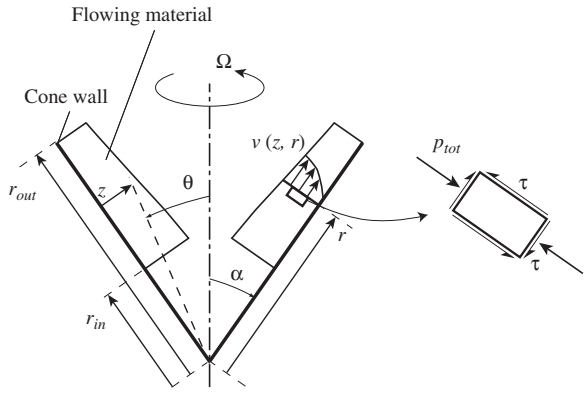

Fig. 4. Model geometry.

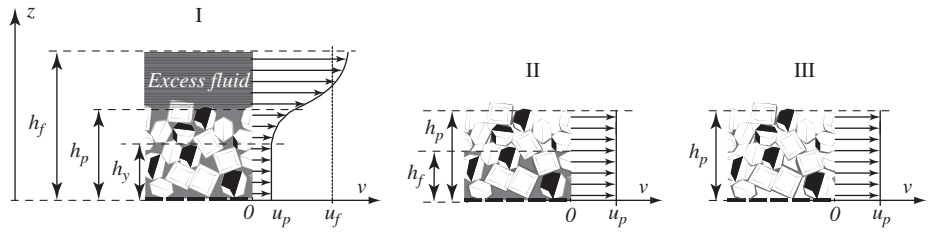

Fig. 3. Microstructure and velocity profile of the solid/liquid/air phases in regions I, II and III. The excess fluid can be pure interstitial fluid (case 1) or a homogeneous mixture of interstitial fluid and powder (case 2).

Analysis is further simplified by assuming that gravity g may be neglected compared to the centripetal acceleration. Given that the three dimensionless groups h/r, Ro and $g/r\Omega^2 \sin\alpha$ are all much less than unity the flow momentum equations may be reduced to the equilibrium statements

$$\frac{\partial p_{tot}}{\partial z} = -\rho g^* \cos\alpha \tag{2}$$

$$\frac{\partial \tau}{\partial z} = -\rho g^* \sin\alpha \tag{3}$$

where p_{tot} and τ are the total normal pressure and shear stress within the flow (see Fig. 4), z the through-thickness co-ordinate ($z \approx r(\alpha-\theta)$ where $z \ll r$ and thus $\partial z = -r\partial\theta$), ρ is the local density and

$$g^* = r\Omega^2 \sin\alpha \tag{4}$$

is the centripetal acceleration. At the free-surface of the flow ($z=h$) $p_{tot} = \tau = 0$ and therefore (2) and (3) reduce to

$$\tau = p_{tot} \tan\alpha \tag{5}$$

throughout the flow thickness at any r.

2.2. Treatment of multi-phase flow

The flow within a conical centrifugal filter may be considered to be a problem of three-phase (gas, liquid and solid) interpenetrating flow. Nigmatulin (1991) provides general equations for the analysis of multi-phase interpenetrating flows and the model presented in this paper fits within this overall framework. However, the typical conditions within a conical centrifugal filter suggest that a number of significant simplifications may be made. Firstly we will only consider steady state (i.e. time invariant) and axi-symmetric conditions for a thin flow of liquid and solid on the surface of a spinning conical screen. The influence of the gas phase (air) on the flow is negligible and therefore only the liquid and solid phases need to be considered. For much of the flow (regions II and III) fluid drainage and sedimentation (settling) of the solid particles means that the solid phase has become a densely packed porous "cake" and soil mechanics methods can therefore be adopted for analysis of deformation and seepage. At inlet (Region I) the flow is still an oversaturated slurry. However, analysis of relative movement of solid and liquid in this two-phase flow is further simplified by consideration of two alternative idealizations: either the flow has already separated into a layer of settled "cake" topped by a layer of pure fluid, or the flow remains a homogeneous slurry in which the rate of particle settlement is negligible.

2.3. Newtonian fluid

For a Newtonian viscous fluid a no-slip condition is assumed at the interface of fluid and cone. The linear centrifugal approximation described above gives a parabolic velocity distribution $v(r,z)$ through the flow thickness identical to the classical Nusselt result for laminar flow down an inclined plane.

$$v(r,z) = \frac{3u_f}{2}\frac{z(2h_f - z)}{h_f^2} \tag{6}$$

where $h_f(r)$ is the fluid thickness and $u_f(r) = (1/h_f)\int_0^{h_f} v(r,z)\,dz$ is the through-thickness averaged radial velocity. The basal shear stress τ is related to the fluid thickness h_f and average velocity u_f via

$$\tau = 3\mu_f \frac{u_f}{h_f} \tag{7}$$

where μ_f is the fluid dynamic viscosity.

2.4. Shear traction at the screen

Industrial conical centrifuges are typically designed so that the granular material tends to slip against the comparatively smooth cone screen rather than sticking and shearing internally. The screen construction may be plates with slotted perforations or "wedge-wire sections" (Fig. 5) where the slot width is significantly less than the mean granule diameter (e.g. 75 μm and 500 μm respectively for a sugar screen and sugar crystals), see e.g. Leung (1998) or Grimwood et al. (2005). Slip ensures that all of the granular product leaves the centrifuge, but it can lead to erosion of the screens (Greig et al., 1984).

In an attempt to obtain an analytical model for the flow of sugar massecuite in a conical centrifugal filter, Swindells (1982) assumed that the shear traction at the interface of powder flow and screen after the colour line (in region III) is pure Coulomb friction. He explained the apparent uniform sliding velocity observed experimentally by a strict equality between the coefficient of friction at the powder/wall interface, b, and the cone slope tan α. Observations by Swindells support the idea that Coulomb friction dominates the shear traction at the wall: if the cone slope is more than a few degrees smaller or larger than the Coulomb friction coefficient b the machine does not work in a satisfactory manner: the powder either sticks to the wall or leaves the basket at high velocity, which causes significant crystal breakage and reduces the drying efficiency. While we acknowledge the importance of Coulomb friction at the wall interface, we have shown (Bizard et al., 2011) that an additional velocity-dependent friction component is required to ensure flow stability. Liquid drainage ensures the constant renewal of a thin liquid film at the powder/wall interface, and shearing of this film generates a velocity-dependent shear traction in addition to the Coulomb friction term, as developed in Bizard et al. (2011). We consequently suggest the following expression for the shear traction acting on the sliding wet powder:

$$\tau = au + bp_{eff} \tag{8}$$

where a is the slip velocity dependency coefficient, u the sliding velocity and p_{eff} the interfacial effective pressure, defined as the difference between total and fluid pressures,

$$p_{eff} = p_{tot} - p_f \tag{9}$$

Note that p_{eff} is the effective normal stress acting within the solid phase or, in this particular case, between the solid phase and the screen wall, as defined by Terzaghi (1960).

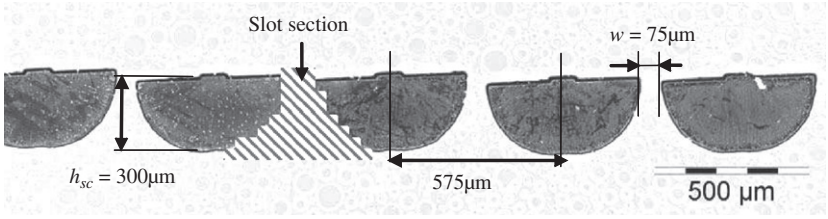

Fig. 5. Section of a typical sugar centrifuge screen.

Yilmazer and co-authors (Yilmazer and Kalyon, 1989; Soltani and Yilmazer, 1998) performed experiments on densely packed suspensions of granular material within a Newtonian fluid and found the viscous slip coefficient a as

$$a \approx \frac{25.0\mu_f}{d_p} \tag{10}$$

where μ_f is the interstitial fluid viscosity and d_p the average particle size. We will use this result for a preliminary validation of this work. For completeness we note that the coefficient a as given by (10) is only valid when the interface particles are completely immersed in liquid, so that this relation may not strictly apply to region III. It is expected that a will decrease in region III due to the reduction in liquid content at the interface. We will however assume that the drain height (i.e. capillary rise height) as defined by Dombrowski and Brownell (1954) is of the same order of magnitude as the mean crystal size, so that a in region III takes the same value given by (10) for regions I and II.

2.5. Yield of granular material

The powder (granular material) is assumed to obey the Mohr–Coulomb yield criterion with negligible cohesion, consistent with the results of Davy et al. (2004) for granular sugar. Below yield the powder is assumed to be effectively rigid. Beyond yield the constitutive response is assumed to be that of a pressure and strain-rate dependent Bingham fluid (as suggested, for example, by Norem et al., 1990) thus

$$\frac{\partial v}{\partial z} = \max\left[0, \frac{\tau - p_{eff}\tan\psi}{\mu_y}\right] \tag{11}$$

where ψ is the internal angle of friction of the material and μ_y is the strain-rate dependency coefficient (equivalent to the dynamic viscosity of a Newtonian fluid). This is an over-stress model whereby the strain rate scales with the stress increment above the shear stress at yield $\tau = p_{eff}\tan\psi$. In agreement with experimental observations we shall limit ourselves to the case where the cone angle α is less than the angle of internal friction of the granular material ψ, but just greater than the angle of friction for contact with the basket screen arctan b, thus

$$b < \tan\alpha < \tan\psi \tag{12}$$

2.6. Sedimentation

Sedimentation of powder in a fluid has been studied extensively, especially in hydraulic and chemical engineering, see e.g. Raudkivi (1967) and Nielsen (1992). In the particular case of a conical centrifugal filter the input slurry typically has a high particle volume fraction so that the classical expression proposed by Stokes in order to estimate the settling velocity of an isolated particle in a fluid is not applicable. Instead, hindered settling is likely to take place, which may be significantly slower than the isolated settling described by Stokes (Nielsen, 1992). Actual settling times for the flow in a spinning cone are difficult to estimate and in this study we will thus consider two extreme, bounding inlet conditions: in a first case settling is assumed sufficiently rapid for all the particles to have settled before the flow reaches the upper, perforated cone; in a second case only minimal initial sedimentation has occurred at inlet $r = r_{in}$ and the particle settling velocity within the suspension is assumed negligible relative to the through-thickness velocity of the fluid due to drainage. In the second case the particles are thus assumed to have the same velocity in the z-direction as the fluid.

2.7. Drainage through screen in regions I and II

In order to drain the fluid out of the powder the cone wall is fitted with a screen, a sheet of metal drilled with numerous slots of width w, leaving an open area n_{sc} on the order of 15%. The screen resistance to flow depends upon the Reynolds number within a slot. If viscous effects are dominant, a Poiseuille plane flow model will be appropriate, if inertial effects dominate, a model using Bernoulli's theorem will be more suitable. In this work we will assume a large predominance of the viscous effects, in agreement with the experimental results of Swindells (1982), so that the volumetric flow rate per unit area normal to the screen q_{sc} is related to the pressure gradient dp/dz and the centripetal acceleration g^* through the screen via:

$$q_{sc} = \frac{k_{sc}}{\mu_f}\left(\frac{dp}{dz} + \rho_f g^* \cos\alpha\right) \tag{13}$$

where k_{sc} is the screen permeability and ρ_f the density of the interstitial fluid. If the slots are significantly deeper than they are wide the flow is similar to a Poiseuille flow between two fixed planes and k_{sc} can be estimated via

$$k_{sc} = \frac{n_{sc} w^2}{12} \tag{14}$$

We note in passing that the through-thickness profile of industrial screen slots is usually not straight but rather widens from the working face to the back face, as shown in Fig. 5. Industrial screens will therefore have a permeability higher than that predicted by (14). In particular, the screen permeability as measured by Swindells (1982) is about twice that predicted by (14).

In the case of a flow through a screen of thickness h_{sc} with a pressure p_{int} at the fluid-wall interface and no pressure at the back face, (13) can be re-written as

$$q_{sc} \equiv \frac{k_{sc}}{\mu_f}\left(\frac{\rho_f g^* h_{sc}\cos\alpha + p_{int}}{h_{sc}}\right) \tag{15}$$

2.8. Seepage through saturated powder

In order to calculate the liquid volumetric flow rate per unit area through a saturated powder layer q_p in regions I and II we will make use of Darcy's (1856) law, which can be written as

$$q_p = \frac{k_p}{\mu_f}\left(\rho_f g^* \cos\alpha + \frac{\partial p}{\partial z}\right) \tag{16}$$

where k_p is the powder permeability. In order to ensure fluid mass conservation the flow rate through the powder and through the screen must be equal ($q_{sc} = q_p$), and this yields p_{int}.

2.9. Surface tension effects

We now consider the flow in region II, where the powder is saturated in its lower part ($z < h_f$) and damp at the surface ($h_f < z < h_p$, where h_p is the thickness of the powder layer, see Fig. 3). Seepage in a semi-saturated powder under gravity g may be significantly different from seepage through a saturated media, see e.g. White et al. (1970) due to surface tension effects. However, we will assume that these effects are negligible under the high centripetal accelerations of a conical continuous centrifuge. The relative importance of body forces to surface tension forces in semi-saturated powder may be given by the Bond number, defined as

$$Bo = \frac{d_p^2 \rho_f \Omega^2 r \sin\alpha\cos\alpha}{\gamma} \tag{17}$$

where γ is the interstitial fluid surface tension. In a typical conical centrifuge *Bo* is of the order of 100, so that surface tension effects can be neglected and seepage still obeys Darcy's law in region II.

2.10. Slurry viscosity

For the second condition at inlet we will consider the flow of a homogeneous slurry (a suspension of liquid and solid particles) flowing over an initially thin layer of sedimented particles. Oliver and Ward (1953) found experimentally that when the solid mass ratio of a slurry does not exceed 30%, the mixture can still be taken as Newtonian, its viscosity depending upon the solid mass ratio. For the particular case of sugar massecuite, Awang and White (1976) and Rouillard and Koenig (1980) showed that for high solid mass ratios (up to 60%) the mixture can still be treated as Newtonian viscous within a practical range of shear rates, the viscosity increasing exponentially with the solid content. We will show that the viscosity of the slurry has only a mild influence on the position of the colour line in a continuous centrifuge, so that considering more complex constitutive models such as the power-law viscous fluid presented by Swindells (1982) is unnecessary.

3. Overview of analysis

A one dimensional analysis is now presented for the flow of a granular solid/liquid mixture within a rotating perforated cone at a constant input flow rate. The analysis assumes that the flow is thin, that the gravitational, convective and Coriolis components of acceleration are negligible compared to the centrifugal action and that the perforated cone angle and surface geometry are such that the granular solid phase tends to slide against its internal surface. These assumptions match the conditions observed in the practical case of a conical centrifuge as used in the sugar industry.

The flow enters the perforated cone at inlet radius r_{in} with a total mass flow rate $\dot{m}$ and a liquid mass fraction M^M_{in}. Because the input material cannot be fed below saturation M^M_{in} is constrained to lie between the following boundaries:

$$\rho_f/[n_p\rho_f+(1-n_p)\rho_p]<M^M_{in}\le 1 \tag{18}$$

where ρ_f and ρ_p are the fluid and solid particle densities and n_p is the dense packed porosity of the powder. For practical values the lower bound for M^M_{in} is about 0.4. As fluid is drained out of the cone through powder and screen the fluid thickness measured from the wall, h_f, decreases until it attains the powder thickness h_p at a radial coordinate r_{CL1} (end of region I, beginning of region II, see Fig. 3). The flow is then that of a damp powder of thickness h_p, the bottom of which is saturated with fluid over a thickness h_f (Region II), until all pores are emptied and a flow of damp powder is left (Region III, starting at radial coordinate r_{CL2}). This flow of damp powder exits at the outlet radius r_{out}, as shown in Fig. 4.

Two cases are considered for the flow at inlet. In a first case the solid particles are all settled before reaching the perforated cone and a layer of pure fluid flows on top of a saturated, densely packed powder layer which is itself sliding on the screen surface. In a second case the slurry is assumed to be a homogeneous suspension at the start of the perforated cone, with little initial settling of powder. In the perforated cone fluid drainage drags the particles down onto the wall and a powder layer builds up gradually. The remaining slurry flows on top of this sliding powder layer and while its thickness decreases through drainage and sedimentation, its moisture content remains at its initial value.

Equilibrium and mass conservation relations are established for each of the regions described in Fig. 3. Ordinary differential equations (ODEs) are obtained for the flow in regions I and II and an algebraic equation, independent of the coordinate r, is obtained for the flow velocity in region III. Key non-dimensional groups are identified and conditions to maximize the length of region III are given.

4. Governing equations

Governing equations are now derived for the flow in regions I–III (see Fig. 2). In a first section yield within the saturated powder layer (regions I and II) is analysed. Equilibrium relations for each layer in the three regions are then established. Finally, fluid and solid mass conservation relations are given for each region. Both fluid and powder are treated as incompressible (with fixed densities and porosity) and with constant constitutive properties throughout the cone. In order to keep as much commonality as possible between the two cases considered at inlet we consider the general case of a two-layer flow in region I: an excess liquid layer of constant liquid volume fraction M^V_{EF} flows on top of a saturated densely packed powder layer. The density of the excess fluid is related to the densities of its components and to its liquid volume fraction via

$$\rho_{EF}=M^V_{EF}\rho_f+(1-M^V_{EF})\rho_p \tag{19}$$

4.1. Stress distribution and yield

In region I the effective pressure at $z=h_p$ is zero since $p_{tot}=p_f$. It is thus clear from (5) and (11) that the powder yields over a finite thickness below the powder layer surface. In contrast, in region II the effective pressure equals the total pressure at the surface of the saturated powder layer ($z=h_f$) and the ratio of shear stress to effective pressure equals $\tan\alpha$—see (5). Since we consider only the case where $\tan\alpha<\tan\psi$ the saturated powder layer is rigid over a finite thickness below its surface. As we assume the powder to be homogeneous the fluid and total pressures vary linearly through the thickness. This implies that the ratio τ/p_{eff} has a first derivative of constant sign, so that this ratio can reach the particular value $\tan\psi$ at most once through the thickness. We conclude that in region I the powder layer yields at its surface, with possibly a rigid layer at its base, while in region II its surface is rigid with the possibility of a yielded layer at the bottom of the flow. Relationships to obtain the through-thickness coordinate of the yield surface h_y are now given for each region.

4.1.1. Region I: fluid layer on top of saturated powder

The fluid pressure varies linearly through the thickness of the homogeneous powder layer and we write this as

$$p_f(r,z)=\rho_f h_p g^*\cos\alpha\left(A^I_f+B^I_f\frac{z-h_p}{h_p}\right)\quad\text{for } 0\le z\le h_p \tag{20}$$

where the dimensionless coefficients A^I_f and B^I_f depend upon r but not upon z. A^I_f and B^I_f are now calculated. In region I (16) reads

$$q_p=\frac{k_p[g^*\cos\alpha(\rho_{EF}h_f+(\rho_f-\rho_{EF})h_p)-p_{int}]}{\mu_f h_p} \tag{21}$$

Mass conservation of the fluid ($q_{sc}=q_p$) dictates equality of (15) and (21); and therefore

$$p_f(r,0)=p_{int}=\frac{g^*h_{sc}\cos\alpha(h_p(k_p(\rho_f-\rho_{EF})-\rho_f k_{sc})+h_f k_p\rho_{EF})}{h_{sc}k_p+h_p k_{sc}} \tag{22}$$

The fluid pressure at $z=h_p$ is given by

$$p_f(r,h_p)=\rho_{EF}g^*\cos\alpha(h_f-h_p) \tag{23}$$

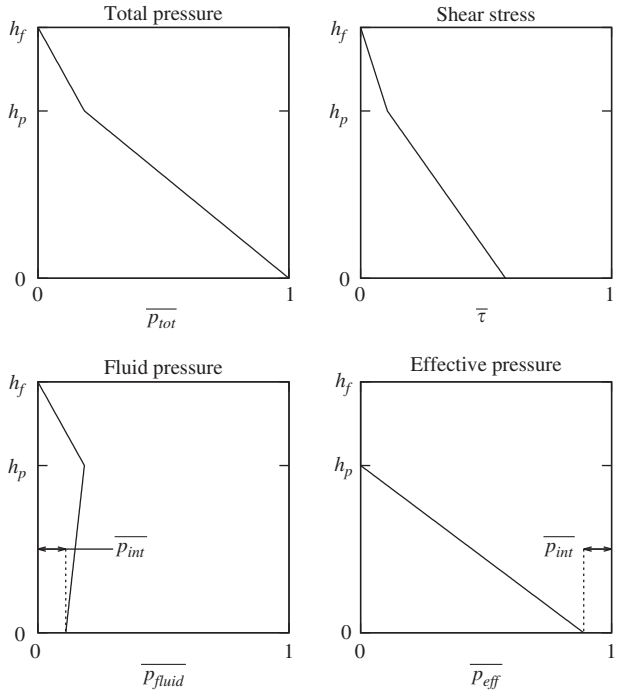

Fig. 6. Region I: typical shear stress and pressure through-thickness profiles, normalized by the maximal total pressure.

Solving (20)–(23) for A_f^{I} and B_f^{I} yields

$$A_f^{\mathrm{I}}(r) = \frac{\rho_{EF}(h_f - h_p)}{\rho_f h_p} \tag{24}$$

$$B_f^{\mathrm{I}}(r) = \frac{k_{sc}[\rho_{EF}(h_f - h_p) + \rho_f h_{sc}] - \rho_f h_{sc} k_p}{\rho_f (h_{sc} k_p + h_p k_{sc})} \tag{25}$$

The total pressure also varies linearly through the thickness, and we write this as

$$p_{tot}(r,z) = \rho_f h_p g^* \cos\alpha (A_f^{\mathrm{I}} + B_{tot}^{\mathrm{I}} \frac{z - h_p}{h_p}) \quad \text{for } 0 \le z \le h_p \tag{26}$$

where the dimensionless coefficient B_{tot}^{I} is independent of z. B_{tot}^{I} is obtained by considering the total weight per unit area at $z=0$ and $z=h_p$:

$$B_{tot}^{\mathrm{I}} = A_f^{\mathrm{I}} - \frac{\rho_{EF}(h_f - h_p) + \rho_{SP} h_p}{\rho_f h_p} \tag{27}$$

where ρ_{SP} is the density of saturated powder

$$\rho_{SP} = n_p \rho_f + (1 - n_p)\rho_p \tag{28}$$

The effective pressure can then be obtained from (9). Typical stress profiles are shown in Fig. 6.

The material yields when the ratio of shear stress to effective pressure exceeds the internal friction coefficient $\tan\psi$, see (11). At $z = h_p$, p_{eff} is zero and a yielded layer of thickness $(h_p - h_y)$ thus exists throughout region I ($r_{in} < r < r_{CL1}$). The through-thickness coordinate above which the material yields h_y is found by solving

$$\tau(r,h_y) = p_{eff}(r,h_y)\tan\psi \tag{29}$$

This is shown graphically in Fig. 7.

Upon making use of (5), (9), (20), (26), (29) yields

$$h_y = \frac{h_p((B_{tot}^{\mathrm{I}} - A_f^{\mathrm{I}})\tan\alpha + (B_f^{\mathrm{I}} - B_{tot}^{\mathrm{I}})\tan\psi)}{(B_f^{\mathrm{I}} - B_{tot}^{\mathrm{I}})\tan\psi + B_{tot}^{\mathrm{I}}\tan\alpha} \tag{30}$$

If the yield criterion (11) is attained at the bottom of the flow then the entire thickness has yielded and (30) reverts to $h_y = 0$. The

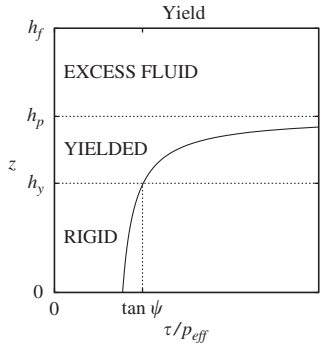

Fig. 7. Region I: typical shear stress to effective pressure ratio within the powder layer.

velocity profile within the yielded region is found by integrating (11). As τ and p_{eff} are linear over the thickness the velocity profile within the yielded region is quadratic. Velocity continuity demands $v(r,h_y) = u_p$, where u_p is the sliding velocity of the underlying rigid layer of powder. The velocity profile can then be written in the form

$$v_y(r,z) = u_p\left(1 + \frac{B_y^{\mathrm{I}}(z - h_y)}{h_p} + \frac{C_y^{\mathrm{I}}\left(z^2 - h_y^2\right)}{h_p^2}\right) \tag{31}$$

where the dimensionless coefficients B_y^I and C_y^I read

$$B_y^{\mathrm{I}}(r) = \frac{g^*\rho_f h_p^2((A_f^{\mathrm{I}} - B_{tot}^{\mathrm{I}})\tan\alpha + (B_{tot}^{\mathrm{I}} - B_f^{\mathrm{I}})\tan\psi)\cos\alpha}{u_p \mu_y} \tag{32}$$

$$C_y^{\mathrm{I}}(r) = \frac{g^*\rho_f h_p^2((B_f^{\mathrm{I}} - B_{tot}^{\mathrm{I}})\tan\psi + B_{tot}^{\mathrm{I}}\tan\alpha)\cos\alpha}{2u_p \mu_y} \tag{33}$$

The velocity within the yielded layer attains its maximum v_{ytop} at $z = h_p$.

4.1.2. Transition between regions I and II: $r = r_{CL1}$

We now consider the start of the colour line ($r = r_{CL1}$). We will show that at this radial coordinate the flow, made up only of saturated powder, is either entirely rigid or entirely yielded. At $r = r_{CL1}$, $h_p = h_f$ and therefore the shear and effective stresses can be written as

$$\tau = p_{tot}(r_{CL1},z)\tan\alpha = \rho_{SP} g^* h_p\left(1 - \frac{z}{h_p}\right)\sin\alpha \tag{34}$$

$$p_{eff} = p_{tot}(r_{CL1},z) - p_f(r_{CL1},z) = [\rho_{SP} g^* h_p \cos\alpha - p_{int}]\left(1 - \frac{z}{h_p}\right) \tag{35}$$

where p_{int} is the fluid pressure at the powder/screen interface, calculated from (22) as

$$p_{int} = \frac{h_{sc} h_p \rho_f g^* \cos\alpha (k_p - k_{sc})}{h_{sc} k_p + h_p k_{sc}} \tag{36}$$

This leads to

$$\frac{\tau}{p_{eff}} = \tan\alpha\left[1 - \frac{p_{int}}{\rho_{SP} g^* h_p \cos\alpha}\right]^{-1} \tag{37}$$

This ratio is independent of the through-thickness coordinate z. We conclude that the layer is either entirely yielded or entirely rigid through its whole thickness at $r = r_{CL1}$. Consider the two following limit cases:

(i) If the screen resistance to drainage is low ($h_{sc} \to 0$, or $k_{sc} \to \infty$) the fluid pressure at $z = 0$ p_{int} vanishes—see (36), and the ratio τ/p_{eff} tends towards $\tan\alpha$. Since we consider the case $\alpha < \psi$ the layer does not yield.

(ii) If however drainage is difficult through the screen ($h_p \to \infty$, or $k_{sc} \to 0$) p_{int} tends towards the static fluid pressure $\rho_f g^* h_p \cos\alpha$ and at $r = r_{CL1}$ the ratio of shear traction to effective pressure tends towards

$$\frac{\tau}{p_{eff}} \to \frac{\rho_{SP}}{\rho_{SP}-\rho_f}\tan\alpha \tag{38}$$

As we consider the case where the densities of the fluid and powder are similar ($\rho_{SP} \approx \rho_f$) the limit value given in (38) tends towards infinity and the layer is fully yielded.

We conclude that in the first case the layer is entirely rigid at $r = r_{CL1}$ and in the second case it is entirely yielded.

4.1.3. Region II: saturated/damp flow

Region II consists of a damp powder layer on top of a saturated powder layer. Above the saturated layer ($z > h_f$) there can be no yield: $p_{eff} = p_{tot}$ and from equilibrium relation (5) we conclude that $\tau/p_{eff} = \tan\alpha$. We consider the case where $\alpha < \psi$ so that the top damp powder layer does not yield.

The fluid pressure in the saturated powder layer can be written as

$$p_f(r,z) = \rho_f g^* \cos\alpha h_f B_f^{II}\left(1-\frac{z}{h_f}\right) \tag{39}$$

where

$$B_f^{II} = \frac{h_{sc}(k_p-k_{sc})}{h_f k_{sc}+h_{sc}k_p} \tag{40}$$

The total pressure reads

$$p_{tot}(r,z) = \rho_f g^* \cos\alpha h_f\left[A_{tot}^{II}+B_{tot}^{II}\left(1-\frac{z}{h_f}\right)\right] \tag{41}$$

where

$$A_{tot}^{II} = \frac{(1-n_p)\rho_p(h_p-h_f)}{\rho_f h_f} \tag{42}$$

$$B_{tot}^{II} = \frac{n_p\rho_f+(1-n_p)\rho_p}{\rho_f} \tag{43}$$

Typical stress profiles are shown in Fig. 8.

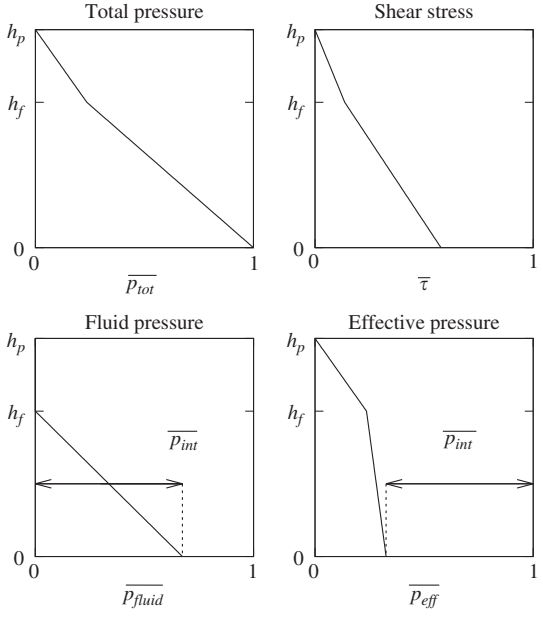

Fig. 8. Region II: typical shear stress and pressure through-thickness profiles, normalized by the maximal total pressure.

In a similar fashion to that outlined for region I we obtain the through-thickness coordinate of the yield surface and the velocity profile in the yielded layer as

$$h_y = \frac{(A_{tot}^{II}+B_{tot}^{II})\tan\alpha-(A_{tot}^{II}-B_f^{II}+B_{tot}^{II})\tan\psi}{(B_f^{II}-B_{tot}^{II})\tan\psi+B_{tot}^{II}\tan\alpha}h_f \tag{44}$$

and

$$v_y(r,z) = u_p\left(1+B_y^{II}\frac{z}{h_f}+C_y^{II}\frac{z^2}{h_f^2}\right) \tag{45}$$

respectively, where

$$B_y^{II} = \frac{\rho_f g^* h_f^2 \cos\alpha[(A_{tot}^{II}+B_{tot}^{II})\tan\alpha-(A_{tot}^{II}-B_f^{II}+B_{tot}^{II})\tan\psi]}{\mu_y u_p} \tag{46}$$

$$C_y^{II} = \frac{\rho_f g^* h_f^2 \cos\alpha[(B_{tot}^{II}-B_f^{II})\tan\psi-B_{tot}^{II}\tan\alpha]}{2\mu_y u_p} \tag{47}$$

In the case where the shear stress τ is less than $p_{eff}\tan\alpha$ at $z=0$ the entire layer is rigid and (44) reverts to $h_y=0$. We note that in region II the rigid layer is flowing at the same velocity as the top of the underlying yielded layer, v_{ytop}. The basal slip velocity is still written as u_p. We note that in the case where there is no yield in the layer, $u_y = u_p = v_{ytop}$.

4.1.4. Region III: after the colour line, flow of damp powder

In region III the powder is damp: the pores are not saturated with liquid and therefore the effective pressure is equal to the total pressure. We conclude from this and (5), (11) that the layer does not yield anywhere in region III.

4.2. Traction equilibrium at the layer interfaces

The shear traction at the fluid/powder interface ($z = h_p$) in region I is obtained from (5) and (7) as

$$3\mu_{EF}\frac{u_f-v_{ytop}}{h_f-h_p} = p_{tot}(r,h_p)\tan\alpha \tag{48}$$

The shear traction at the powder/screen interface throughout the cone is represented by (8). Upon making use of (5) we obtain the equilibrium relation at the wall as

$$au_p + bp_{eff}(r,0) = p_{tot}(r,0)\tan\alpha \tag{49}$$

This relation is assumed to hold for regions I–III.

In region III the effective pressure and the total pressure at the wall share the same value:

$$p_{eff}(r,0) = p_{tot}(r,0) = \rho_p(1-n_p)g^* h_p \cos\alpha \quad \text{for } r > r_{CL2} \tag{50}$$

4.3. Mass conservation relations

We now consider solid and fluid mass conservation in the flow. For all regions powder losses through the screen are neglected, in agreement with experimental observations (Swindells, 1982). In contrast, fluid drainage in regions I and II leads to a loss of fluid within the basket. Mass conservation relations are now given for both the powder and the fluid in each flow regions I–III.

4.3.1. Region I

Consider volume conservation in the circular element of radial width dr and perimeter $2\pi r \sin\alpha$ located at a radial coordinate r shown in Fig. 9. Seepage in the radial direction is assumed negligible and the volumetric flow rate of liquid entering this

element is therefore (Fig. 10)

$$Q^{I}_{convective}(r) = 2\pi r \sin\alpha(M^{V}_{EF}(h_f - h_p)u_f + n_p[h_y u_p + (h_p - h_y)u_y]) \quad (51)$$

where u_y is the average radial velocity within the yielded region, obtained from (31) as

$$u_y = \frac{(2C^{I}_y - 3B^{I}_y)h_p h_y + (3B^{I}_y + 2C^{I}_y + 6)h_p^2 - 4C^{I}_y h_y^2}{6h_p^2} u_p \quad (52)$$

The volumetric flow rate of liquid seeping out of the same element and through the screen is calculated from (21), (22) as

$$dQ^{I}_{seepage} = \frac{2\pi k_p k_{sc} r g^* \sin\alpha \cos\alpha(\rho_f(h_{sc} + h_p) + \rho_{EF}(h_f - h_p))}{\mu_f(k_p h_{sc} + h_p k_{sc})} dr \quad (53)$$

Upon making use of (51)–(53), we obtain the fluid mass conservation relation as a non-linear ordinary differential equation (ODE) in r:

$$\frac{d}{dr}[Q^{I}_{convective}] + \frac{dQ^{I}_{seepage}}{dr} = 0 \quad (54)$$

The associated initial condition is given by the flow rate of fluid at inlet:

$$\rho_f Q^{I}_{convective} = M^{M}_{in}\dot{m} \quad \text{at } r = r_{in} \quad (55)$$

Powder losses through the screen are neglected and the input mass flow rate of particles, $(1-M^{M}_{in})\dot{m}$, is therefore conserved. At any coordinate r in region I the total flow rate of powder is the sum of the solid mass flow rate within each of the layers, and we write this as:

$$2\pi\rho_p r \sin\alpha[(1-n_p)[h_y u_p + (h_p - h_y)u_y] + (1-M^{V}_{EF})(h_f - h_p)u_f] = (1-M^{M}_{in})\dot{m} \quad (56)$$

Region I ends when $h_f = h_p$, at the radial coordinate $r = r_{CL1}$.

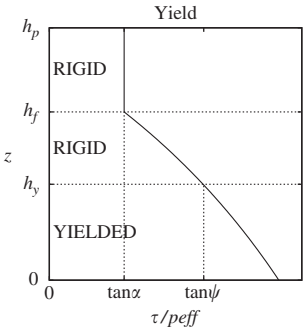

Fig. 9. Region II: typical shear stress to effective pressure ratio within the powder layer.

4.3.2. Region II

Solid mass conservation in region II dictates

$$2\pi\rho_p r \sin\alpha(1-n_p)[(h_p - h_y)v_{ytop} + h_y u_y] = (1-M^{M}_{in})\dot{m} \quad (57)$$

The initial condition is given by $h_f = h_p$ at $r = r_{CL1}$.

The liquid flow rate out of the element of width dr at the coordinate r shown in Fig. 11 is

$$dQ^{II}_{seepage} = \frac{2\pi\rho_f k_p k_{sc}(h_f + h_{sc}) r g^* \cos\alpha \sin\alpha}{\mu_f(k_p h_{sc} + h_f k_{sc})} dr \quad (58)$$

and transport of fluid via the radial displacement of yielded and rigid saturated layers leads to the following convective volumetric

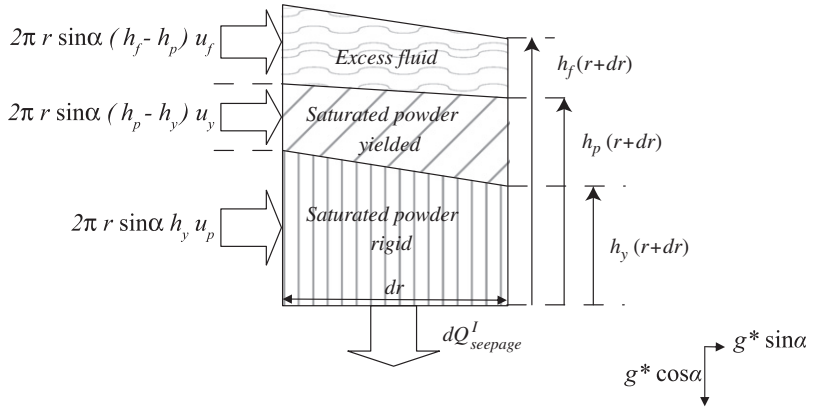

Fig. 10. Region I: volume fluxes through a control volume of width $2\pi r \sin\alpha$ and length dr subjected to a local gravity of amplitude $g^* = r\Omega^2 \sin\alpha$.

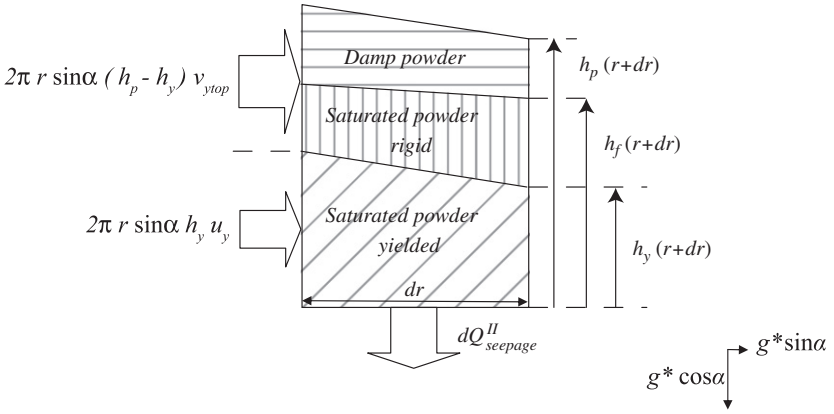

Fig. 11. Region II: volume fluxes through a control volume of width $2\pi r \sin\alpha$ and length dr subjected to a local gravity of amplitude $g^* = r\Omega^2 \sin\alpha$.

flow rate:

$$Q^{II}_{convective}(r) = 2\pi n_p r((h_f - h_y)v_{ytop} + h_y u_y)\sin\alpha \tag{59}$$

Fluid conservation in the element of the saturated layer shown in Fig. 11 then yields the ODE

$$\frac{d}{dr}[Q^{II}_{convective}] + \frac{dQ^{II}_{seepage}}{dr} = 0 \tag{60}$$

4.3.3. Region III

In region III (57) still holds with $h_y = 0$ and $u_y = v_{ytop} = u_p$. Eqs. (49), (50), (57) lead to algebraic expressions for h_p and u_p,

$$h_p = \frac{1}{r\Omega\sin\alpha}\left(\frac{a(1-M^M_{in})\dot{m}}{2\pi(1-\hat{b})(1-n_p)^2\rho_p^2\sin\alpha}\right)^{1/2} \tag{61}$$

$$u_p = \Omega\sin\alpha\left(\frac{(1-\hat{b})(1-M^M_{in})\dot{m}}{2\pi a\sin\alpha}\right)^{1/2} \tag{62}$$

where $\hat{b}$ is the ratio of the powder/screen coefficient of friction to the cone slope,

$$\hat{b} = \frac{b}{\tan\alpha} \tag{63}$$

Note that the flow velocity u_p is independent of position r in region III.

4.4. Inlet conditions and flow properties in region I

Depending upon the proportion of particles that are sedimented at inlet the volumetric fluid ratio M^V_{EF} of the top liquid layer could, in theory, vary between limits of 1 (fully settled flow) and $\rho_p M^M_{in}/(\rho_p M^M_{in} + \rho_f(1-M^M_{in}))$ (no initially settled particles). Two different cases which approximate these limits are considered for the flow conditions at inlet.

4.4.1. Case 1: fully settled flow at inlet

In case 1 the powder is assumed to be fully settled at inlet, so that the top layer in region I does not contain any particles. This leads to the following values for the fluid layer properties:

$$M^V_{EF} = 1 \tag{64}$$

$$\mu_{EF} = \mu_f \tag{65}$$

4.4.2. Case 2: homogeneous slurry with small initial settlement

In case 2 most of the particles are still in homogeneous suspension in the fluid with only minimal initial settlement so that $\rho_p M^M_{in}/(\rho_p M^M_{in} + \rho_f(1-M^M_{in})) < M^V_{EF} < 1$. The sliding friction model (8) can be considered sound provided at least a minimally thin, rigid cake has settled. We consequently assume as a minimum that a layer two particles thick has settled at the inlet:

$$h_p = 2d_p \quad \text{at } r = r_{in} \tag{66}$$

$$\mu_{EF} = \mu_{sl} \tag{67}$$

where the slurry viscosity μ_{sl} may be obtained from the measurements of Awang and White (1976) and Rouillard and Koenig (1980). In this model the settling velocity of particles is neglected compared to the fluid velocity in the through-thickness direction. M^V_{EF} is thus constant throughout the top layer in region I and depends upon the amount of powder that has already settled at inlet. The value of M^V_{EF} can be found by solving (30), (31), (48), (49), (52), (55), (56), (66), (67) at inlet ($r = r_{in}$).

5. Non-dimensional approach

The powder slip velocity u_p (62) in region III is independent of r and therefore provides a convenient reference value:

$$u_{ref} \equiv \Omega\sin\alpha\left(\frac{(1-M^M_{in})\dot{m}(1-\hat{b})}{2\pi a\sin\alpha}\right)^{1/2} \tag{68}$$

Eq. (61) is evaluated at $r = r_{in}$ in order to obtain a corresponding reference value for the flow thickness:

$$h_{ref} \equiv \frac{1}{r_{in}\Omega\sin\alpha}\left(\frac{a(1-M^M_{in})\dot{m}}{2\pi(1-\hat{b})(1-n_p)^2\rho_p^2\sin\alpha}\right)^{1/2} \tag{69}$$

Upon making use of (68), (69) we define the following dimensionless groups:

(i) the dimensionless radial coordinate R

$$R \equiv \frac{r}{r_{in}} \tag{70}$$

(ii) the dimensionless thicknesses H_f, H_p, H_{sc}, H_y

$$H_f \equiv \frac{h_f}{h_{ref}}, \quad H_p \equiv \frac{h_p}{h_{ref}}, \quad H_{sc} \equiv \frac{h_{sc}}{h_{ref}}, \quad H_y \equiv \frac{h_y}{h_{ref}} \tag{71}$$

(iii) the dimensionless velocities U_f, U_p, U_y, V_y^{top}

$$U_f \equiv \frac{u_f}{u_{ref}}, \quad U_p \equiv \frac{u_p}{u_{ref}}, \quad U_y \equiv \frac{u_y}{u_{ref}}, \quad V_{ytop} \equiv \frac{v_{ytop}}{u_{ref}} \tag{72}$$

(iv) the slenderness ratio $\hat{H}$

$$\hat{H} \equiv \frac{h_{ref}}{r_{in}}\cot\alpha \tag{73}$$

(v) the Reynolds number P

$$P \equiv \frac{\rho_p u_{ref} h_{ref}}{\mu_f} \tag{74}$$

(vi) the density ratio $\overline{\rho}$, which will always be larger than unity in this analysis,

$$\overline{\rho} \equiv \frac{\rho_p}{\rho_f} \tag{75}$$

(vii) the viscosity number $\hat{a}$

$$\hat{a} \equiv \frac{a h_{ref}}{3(1-n_p)(1-\hat{b})\overline{\rho}\mu_f} \tag{76}$$

(viii) the seepage number Z,

$$Z \equiv \frac{k_p\rho_f\Omega^2 r_{in}^2\sin\alpha\cos\alpha}{\mu_f h_{ref} u_{ref}} = \frac{2\pi\Omega^2\rho_f\rho_p k_{sc}(1-n_p)r_{in}^3\sin^2\alpha\cos\alpha}{(1-M^M_{in})\mu_f\dot{m}} \tag{77}$$

(ix) the permeability ratio κ

$$\kappa \equiv \frac{k_{sc}}{k_p} \tag{78}$$

(x) The relative viscosity of the yielded paste $\overline{\mu}_y$

$$\overline{\mu}_y \equiv \frac{\mu_y}{\mu_f} \tag{79}$$

(xi) Following Rouillard and Koenig (1980) we define the relative viscosity of the slurry $\overline{\mu}_{sl}$ as

$$\overline{\mu}_{sl} \equiv \frac{\mu_{sl}}{\mu_f} \tag{80}$$

(xii) We write the relative viscosity of the top fluid layer in region I as

$$\overline{\mu_{EF}} \equiv \frac{\mu_{EF}}{\mu_f} \tag{81}$$

(xiii) The dimensionless particle size D_p is defined as

$$D_p = \frac{d_p}{h_{ref}}. \tag{82}$$

Note that $1/D_p$ gives the thickness in number of particles of a layer of reference thickness h_{ref}.

The Rossby number can be written as a function of the dimensionless groups defined above:

$$Ro \equiv \frac{u_{ref}}{r_{in}\Omega \sin\alpha} = \sqrt{\frac{P\hat{H}\tan\alpha}{3\overline{\rho}\hat{a}}} \tag{83}$$

Note that for the slender flow centrifugal approximation (2)–(5) to hold both Ro and $\hat{H}$ must be significantly smaller than unity (Bizard et al., 2011). Upon using (69)–(82) we can re-write the governing equations for each region of the cone.

5.1. Region I

The dimensionless parameters A_f^{I}, B_f^{I}, A_{tot}^{I}, B_{tot}^{I}, A_y^{I}, B_y^{I} can be re-expressed as

$$A_f^I = \frac{(\overline{\rho}-M_{EF}^V(\overline{\rho}-1))(H_f-H_p)}{H_p} \tag{84}$$

$$B_f^I = \frac{\kappa(H_f-H_p)(\overline{\rho}-M_{EF}^V(\overline{\rho}-1))+(\kappa-1)H_{sc}}{\kappa H_p+H_{sc}} \tag{85}$$

$$B_{tot}^I = \frac{H_p(A_f^{\mathrm{I}}-(\overline{\rho}-1)(M_{EF}^V-n_p))+H_f(M_{EF}^V(\overline{\rho}-1)-\overline{\rho})}{H_p} \tag{86}$$

$$B_y^I = \frac{3R\hat{a}H_p^2[(B_{tot}^{\mathrm{I}}-B_f^{\mathrm{I}})\tan\psi\cot\alpha+(A_f^{\mathrm{I}}-B_{tot}^{\mathrm{I}})]}{\overline{\mu_y}U_p} \tag{87}$$

$$C_y^I = \frac{3R\hat{a}H_p^2\cot\alpha((B_f^{\mathrm{I}}-B_{tot}^{\mathrm{I}})\tan\psi+B_{tot}^{\mathrm{I}}\tan\alpha)}{2\overline{\mu_y}U_p} \tag{88}$$

Yield surface (30)

$$H_y = \frac{(B_{tot}^I-B_f^I)\tan\psi+(A_f^I-B_{tot}^I)\tan\alpha}{(B_{tot}^I-B_f^I)\tan\psi-B_{tot}^I\tan\alpha}H_p \tag{89}$$

Through-thickness averaged velocity within the yielded layer (from (31))

$$U_y = \frac{U_p((2C_y^{\mathrm{I}}-3B_y^{\mathrm{I}})H_pH_y+(3B_y^{\mathrm{I}}+2C_y^{\mathrm{I}}+6)H_p^2-4C_y^{\mathrm{I}}H_y^2)}{6H_p^2} \tag{90}$$

Maximum velocity within the yielded layer (from (31))

$$V_{ytop} = \frac{(B_y^{\mathrm{I}}+C_y^{\mathrm{I}}+1)H_p^2-B_y^{\mathrm{I}}H_pH_y-C_y^{\mathrm{I}}H_y^2}{H_p^2}U_p \tag{91}$$

Fluid equilibrium (48)

$$(H_f-H_p)^2R\hat{a}(M_{EF}^V(\overline{\rho}-1)-\overline{\rho})+\overline{\mu_{EF}}(U_f-V_{ytop})=0 \tag{92}$$

Solid equilibrium (49)

$$RH_p(B_f^I\hat{b}-A_f^I+(1-\hat{b})B_{tot}^I)+(1-\hat{b})(1-n_p)\overline{\rho}U_p=0 \tag{93}$$

Fluid conservation (54)

$$\frac{R^2Z\kappa((\overline{\rho}(1-M_{EF}^V)+M_{EF}^V)H_f-(1-M_{EF}^V)(\overline{\rho}-1)H_p+H_{sc})}{\kappa H_p+H_{sc}} + \frac{d}{dR}[R[n_p((H_p-H_y)U_y+H_yU_p)+M_{EF}^V(H_f-H_p)U_f]]=0 \tag{94}$$

Solid conservation (56)

$$R(1-M_{EF}^V)(H_f-H_p)U_f+(1-n_p)[R[(H_p-H_y)U_y+H_yU_p]-1]=0 \tag{95}$$

5.1.1. Inlet conditions for the two limit cases

Case 1: Fully settled flow at inlet. (64) is already dimensionless and (65) can be re-written as

$$\hat{\mu_{EF}} = 1 \tag{96}$$

Case 2: Homogeneous slurry with small initial settlement. Eqs. (66) and (67) can be re-written as

$$H_p = 2D_p \quad \text{at } R=1 \tag{97}$$

$$\hat{\mu_{EF}} = \hat{\mu_s} \tag{98}$$

Region I ends when $H_f=H_p$, at the dimensionless coordinate $R=R_{CL1}$.

5.2. Region II

The dimensionless parameters (B_f^{II}, A_{tot}^{II}, B_{tot}^{II}, B_y^{II}, C_y^{II}) can be re-written as a function of the dimensionless parameters (69)–(82) as

$$B_f^{\mathrm{II}} = \frac{(1-\kappa)H_{sc}}{\kappa H_f+H_{sc}} \tag{99}$$

$$A_{tot}^{\mathrm{II}} = -\frac{(1-n_p)\overline{\rho}(H_f-H_p)}{H_f} \tag{100}$$

$$B_{tot}^{\mathrm{II}} = n_p+\overline{\rho}(1-n_p) \tag{101}$$

$$B_y^{\mathrm{II}} = \frac{3R\hat{a}H_f^2[(A_{tot}^{\mathrm{II}}+B_{tot}^{\mathrm{II}})\cot\psi-\cot\alpha(A_{tot}^{\mathrm{II}}-B_f^{\mathrm{II}}+B_{tot}^{\mathrm{II}})]}{\overline{\mu}U_p} \tag{102}$$

$$C_y^{\mathrm{II}} = \frac{3R\hat{a}H_f^2((B_{tot}^{\mathrm{II}}-B_f^{\mathrm{II}})\cot\alpha\tan\psi-B_{tot}^{\mathrm{II}})}{2\overline{\mu}U_p} \tag{103}$$

Through-thickness coordinate of the yield surface (44)

$$H_y = \frac{H_f((A_{tot}^{\mathrm{II}}+B_{tot}^{\mathrm{II}})\tan\alpha-\tan\psi(A_{tot}^{\mathrm{II}}-B_f^{\mathrm{II}}+B_{tot}^{\mathrm{II}}))}{(B_f^{\mathrm{II}}-B_{tot}^{\mathrm{II}})\tan\psi+B_{tot}^{\mathrm{II}}\tan\alpha} \tag{104}$$

Average velocity through the yielded thickness

$$U_y = \frac{U_p(3B_y^{\mathrm{II}}H_fH_y+2C_y^{\mathrm{II}}H_y^2+6H_f^2)}{6H_f^2} \tag{105}$$

Velocity at the yield interface

$$V_{ytop} = U_p\left(\frac{B_y^{\mathrm{II}}H_y}{H_f}+\frac{C_y^{\mathrm{II}}H_y^2}{H_f^2}+1\right) \tag{106}$$

Layer equilibrium (49)

$$RH_f\left(A_{tot}^{II}-B_f^{II}\frac{\hat{b}}{1-\hat{b}}+B_{tot}^{II}\right)-(1-n_p)\overline{\rho}U_p=0 \tag{107}$$

Fluid conservation (60)

$$\frac{R^2Z\kappa(H_f+H_{sc})}{n_p(\kappa H_f+H_{sc})}+\frac{d}{dR}[R((H_f-H_y)V_{ytop}+H_yU_y)]=0 \tag{108}$$

Solid mass conservation (57)

$$-RH_p(R)V_{ytop}(R)-RH_y(R)(U_y(R)-V_{ytop}(R))+1=0 \tag{109}$$

Region II ends at $R=R_{CL2}$, when $H_f=0$

5.3. Region III

Upon making use of (61), (69)–(70) we obtain the algebraic expressions for H_p and U_p in region III as

$$H_p=\frac{1}{R} \tag{110}$$

$$U_p=1 \tag{111}$$

respectively.

6. Numerical results and preliminary validation

A typical conical centrifugal filter used in the refinement of beet sugar has been observed in operation by the authors. The centrifuge was operating with the parameters listed in Table 1 with the colour line observed to lie at approximately one third of the cone height (i.e. $R_{CL2}\approx 1.3$).

Use of a stroboscopic light to illuminate the flow of the granular sugar above the colour line (in region III) revealed the radial velocity to be of the order of 0.1 m/s. The values in Table 1 are used as a base for numerical illustration and provide a preliminary validation of the model. Upon making use of these values (10) and (14) yield $a=5\times10^4$ kPa s m^{-1} and $k_{sc}=9.1\times10^{11}$ m^2 respectively. The reference values for flow velocity and thickness at inlet are obtained using (68) and (69): $u_{ref}=0.15$ m/s and $h_{ref}=11.9$ mm. This value of the reference sliding velocity is in close agreement with the observed estimated granular velocity. The dimensionless groups resulting from the values given in Table 1 are given in Table 2.

Also included in Table 2 are the minimum value for the Bond number $Bo(r_{in})$ and the maximum value of the Rossby number $Ro(r_{out})$. We note that, consistent with the model assumptions, $Bo\gg1$ and $Ro\ll1$ everywhere in the cone. The system of equations (89)–(95), (104)–(109), along with (64), (96) for case 1 and (97), (98) for case 2, is solved for the eight unknowns (H_f, H_p, H_y, U_f, U_p, U_y, V_{ytop}, M_{EF}^V) in each region. The solutions are found numerically making use of the NDSolve function of Mathematica 7.0 Wolfram Research (2008). Dimensionless flow thickness and velocity distributions through the cone are plotted in Figs. 12 and 13. While the initial conditions are significantly different for cases 1 and 2, the colour line (region II) lies at a very similar location in the basket: $R_{CL2}=1.38$ for case 1 and $R_{CL2}=1.36$ for case 2. These predictions are in very close agreement with the experimentally observed position of the colour line. The powder thickness increases sharply within region II, and we interpret this as follows. The decrease in fluid content reduces buoyancy and consequently increases the basal friction via the Coulomb friction term of (8), which slows the flow down and significantly increases the thickness of the flowing damp powder. We note that the predicted variation in surface velocity of the flow throughout the cone (decelerating before the colour line and constant afterwards) is in close agreement with the experimental measurements of Swindells (1982).

7. Discussion

The analytical model developed above can be used for design and optimization of continuous conical centrifuges for a wide range of applications. A minimum requirement for a continuous

Table 1
Parameters considered for a typical sugar centrifuge.

Cone				**Fluid**		
r_{in} (m)	r_{out} (m)	Ω (rad s^{-1})	α (deg)	ρ_f (kg m^{-3})	μ_f (Pa s)	γ (mN m^{-1})
0.54	1.185	1800	30	1400	1	50
Screen				**Input slurry**		
h_{sc} (μm)	n_{sc} (%)	w (μm)		$\dot{m}$ (kg s^{-1})	M_{in}^M (%)	μ_{sl} (Pa s)
300	13	75		5.6	50.	100
Powder						
ρ_p (kg m^{-3})	d_p (μm)	n_p (%)	b	k_p (m^2)	Ψ (deg)	μ_y (Pa s)
1580	500	40	0.5	5×10^{-10}	35	1000

Table 2
Dimensionless parameters for the typical sugar centrifuge described in Table 1.

$\hat{H}$	R_{out}	$\hat{b}$	$\overline{\mu}_{sl}$	$\overline{\mu}_y$	D_p	P
0.04	2.2	0.87	100	1000	0.04	2.7
Z	κ	$\hat{a}$	$\overline{\rho}$	H_{sc}	$Ro(r_{out})$	$Bo(r_{in})$	N_{cap}
1.8	0.18	2200	1.1	0.025	0.0013	60	23

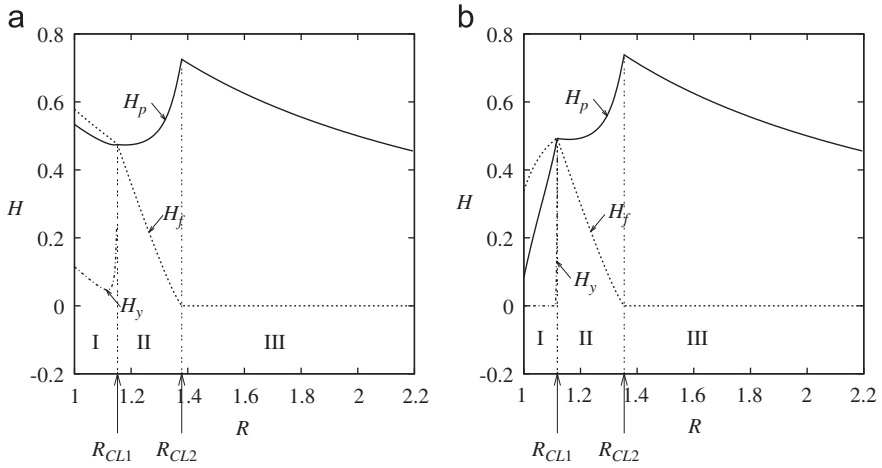

Fig. 12. Typical solutions of the three systems of equations for H_f and H_p within the entire cone for the typical values given in Table 2 for (a) Case 1 and (b) Case 2 of region I.

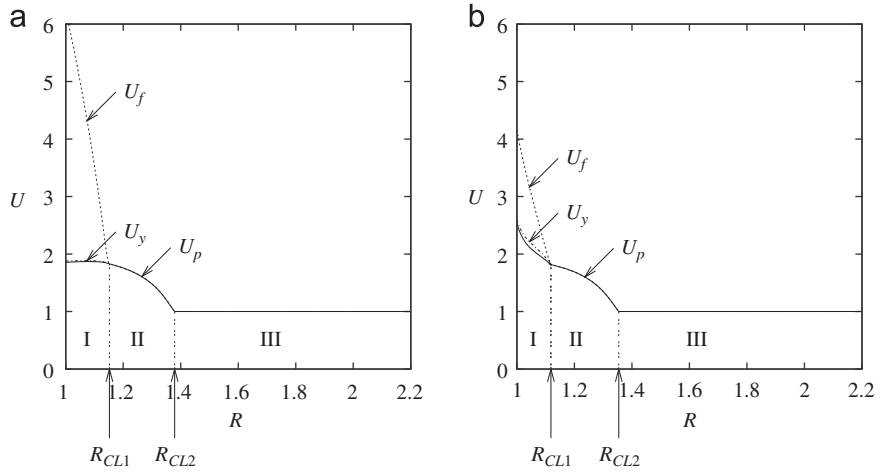

Fig. 13. Typical solutions of the three systems of equations for U_f and U_p within the entire cone for the typical values given in Table 2 for (a) Case 1 and (b) Case 2 of region I.

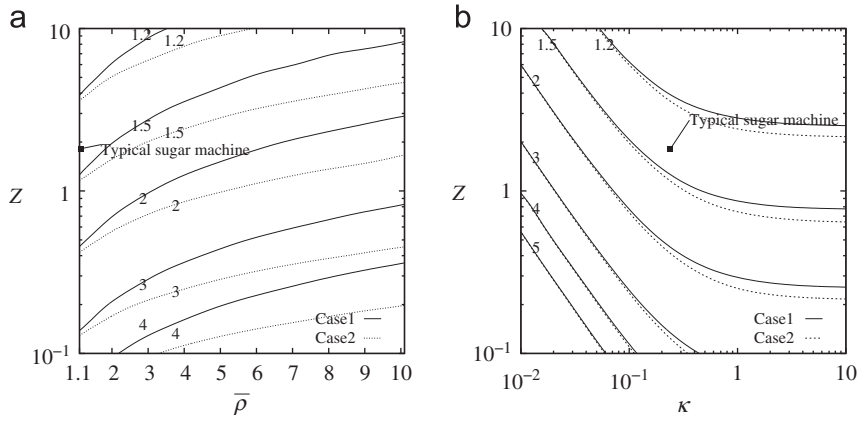

Fig. 14. R_{CL2} contours in the (a) ($\overline{\rho}$, Z) and (b) (κ, Z) plane for the typical values given in Table 2 for inlet cases 1 and 2.

centrifugal is that the flow at outlet is at least desaturated, i.e. it carries only a minimal residual liquid content. This requires that the colour line terminates within the cone $R_{CL2} < R_{out}$. For this reason we shall focus on the position where the colour line ends, R_{CL2}. We now study the relative importance of the dimensionless groups for the performance of the machine.

7.1. Sensitivity of R_{CL2} to dimensionless parameters

The sensitivity of R_{CL2} to key dimensionless parameters is explored around the typical operating point defined by Table 2. Firstly, note that not all dimensionless groups defined earlier appear in the governing equations (48)–(111). In particular, the

slenderness ratio $\hat{H}$, the Reynolds number P and the cone angle α do not influence the position of the colour line. For case 1, the change ΔR_{CL2} of R_{CL2} when a parameter X is changed by ΔX is given by

$$\frac{\Delta R_{CL2}}{R_{CL2}} = -0.28\frac{\Delta Z}{Z} + 0.20\frac{\Delta\overline{\rho}}{\overline{\rho}} + 0.15\frac{\Delta\kappa}{\kappa} + 0.089\frac{\Delta\hat{b}}{\hat{b}} - 0.080\frac{\Delta n_p}{n_p} + 0.069\frac{\Delta H_{sc}}{H_{sc}} \quad (112)$$

Numerical experimentation shows that the only parameter that differs between the two inlet cases, the dimensionless slurry viscosity $\overline{\mu_s}$, has a negligible influence on the colour line position in case 2. We conclude that the constitutive model chosen for the slurry is sufficient for this analysis, and that choosing a power-law constitutive model, as proposed by Swindells (1982), only adds unnecessary complication.

The sensitivity to the dominant parameters is shown graphically in Fig. 14. Use of these maps allows the consequences of a change in design on the position of the end of the colour line (R_{CL2}) to be quickly assessed.

7.2. Drying efficiency

Wakeman (1977) and Tarleton and Wakeman (2007) have shown experimentally that the drying efficiency of a batch centrifuge of radius r_{batch} is closely related to the value of the capillary number N_{cap}, defined as

$$N_{cap}(r_{batch}) = \frac{k_p\rho_f\Omega^2 r_{batch}}{\gamma} \quad (113)$$

We note in passing that the capillary number N_{CAP} can be related to the Bond number Bo, see Section 2.9, and the powder porosity n_p, via the Carman–Kozeny relation (Carman, 1956). In the case of a conical continuous centrifuge we assume the relevant capillary number to estimate the final dryness is taken at outlet,

$$N_{CAP}(r_{out}) = \frac{k_p\rho_f\Omega^2 r_{out}\sin\alpha\cos\alpha}{\gamma} \quad (114)$$

Industrial experience shows that for a machine of fixed size running at constant angular velocity the moisture content at outlet does not depend on the flow rate (Grimwood, 2007). We relate this to our result as follows: an increase in mass flow rate increases the dominant dimensionless parameter Z and thus moves the colour line up the cone, see (112). The time spent by the damp powder in region III is thus reduced, but this does not influence the final moisture content. We conclude that the final moisture content in a continuous centrifuge only depends upon $N_{CAP}(r_{out})$, with the (obvious) condition that the colour line ends before outlet ($R_{CL2} < R_{out}$). For a given application it is thus possible to adjust the moisture content at outlet via the centripetal acceleration at outlet, $\Omega^2 r_{out}\sin\alpha$.

8. Concluding remarks

This paper provides a framework for the analysis of drying flow of wet granular material in a conical centrifugal filter. A one dimensional model of the steady state axisymmetric flow in a spinning perforated cone has been developed. Upon making use of the presented relations it is possible to assess the influence of a change in operating parameters on the performance of a machine. Another application of these results is the development of a continuous conical centrifuge for a new product. Such a development would only require the knowledge of easily measurable quantities such as the Coulomb friction coefficient of the solid against the wall, its density and that of the fluid.

Nomenclature

Roman symbols

Bo	Bond number
C	particles concentration; Dimensionless function of r independent of z
$\hat{H}$	slenderness ratio
H_f	dimensionless fluid thickness
H_p	dimensionless powder thickness
H_y	dimensionless coordinate of the yielded/rigid layers boundary
H_{sc}	dimensionless screen thickness
M_{in}^M	interstitial fluid (moisture) mass fraction in the input slurry
M_{EF}^V	interstitial fluid (moisture) volumetric fraction in the excess fluid
N_{cap}	Capillary number
P	Reynolds number
R	dimensionless radial coordinate
Ro	Rossby number
U_f	dimensionless through-thickness averaged fluid radial velocity
U_p	dimensionless through-thickness averaged powder radial velocity within the rigid layer
U_y	dimensionless through-thickness averaged powder radial velocity within the yielded layer
V_y^{top}	dimensionless radial velocity at the top of the yielded layer
X	arbitrary parameter
Z	dimensionless seepage number
a	slip velocity dependency coefficient of shear traction at the wall
$\hat{a}$	dimensionless slip velocity dependency
b	coefficient of friction for powder against the screen
$\hat{b}$	ratio of the coefficient of friction b to the cone slope $\tan\alpha$
g	earth gravity (g=9.8 m s^{-2})
h	thickness
h_f	thickness of the fluid layer measured from z=0
h_p	thickness of the powder layer
k_p	powder permeability
k_{sc}	screen permeability
n_p	powder porosity
n_{sc}	screen relative open area
p_{eff}	effective pressure
p_{int}	fluid pressure at the flow/screen interface
p_{tot}	total pressure
q_p	volumetric flow rate of liquid per unit area through powder
r	radial coordinate in a spherical coordinate system
r_{in}	inlet radius of the cone (spherical coordinate system)
r_{out}	outlet radius of the cone (spherical coordinate system)
u	average flow velocity
u_f	through-thickness averaged fluid radial velocity
u_p	through-thickness averaged powder radial velocity within the rigid layer
u_y	through-thickness averaged powder radial velocity within the yielded layer
v	local radial velocity

Greek symbols

α	cone semi-angle from the cone axis
ΔX	change in parameter X

γ	interstitial fluid surface tension
κ	permeability ratio
μ_f	interstitial fluid dynamic viscosity
μ_y	strain-rate dependency friction coefficient of yielded powder
$\overline{\mu}_y$	dimensionless strain-rate dependency friction coefficient of yielded powder
μ_{sl}	slurry dynamic viscosity
$\overline{\mu}_{sl}$	ratio of the slurry viscosity to that of the fluid
Ω	cone angular velocity
ϕ	hoop angle
ψ	internal angle of friction of the powder
ρ	density
$\overline{\rho}$	ratio of the powder density to that of the fluid
ρ_f	fluid density
ρ_p	powder density
ρ_{SP}	saturated powder density
τ	shear traction
θ	polar angle

Glossary

cake	densely packed granular material in a centrifuge
colour line	in the basket of a conical centrifuge, region where the flow comprises a top damp layer and a bottom saturated layer
slurry	fluid containing a high volume fraction of solid particles

Acknowledgements

The authors are grateful to the Ashby Scholarship Fund and the Cambridge European Trust for financial support.

References

Awang, M., White, E.T., 1976. Effect of crystal on the viscosity of massecuites. In: Proceedings of the 43rd Conference—Queensland Society of Sugar Cane Technologists, pp. 263–270.

Bizard, A.F.M., Symons, D.D., Fleck, N.A., Durban, D., 2011. Flow of damp powder in a rotating impervious cone. J. Appl. Mech. 78.

Bruin, S., 1969. Velocity distributions in a liquid film flowing over a rotating conical surface. Chem. Eng. Sci. 24, 1647.

Carman, P.C., 1956. Viscous flow: unconsolidated beds. In: Flow of Gases through Porous MediaButterworths Scientific Publications, London (Chapter 1).

Darcy, H., 1856. Determination des lois d'ecoulement de l'eau à travers le sable. In: Les Fontaines Publiques de la Ville de Dijon.

Davy, C.A., Bolton, M.D., Fleck, N.A., 2004. The shearing behaviour of a sugar aggregate. Acta Mater. 52, 3587–3601.

Dombrowski, H.S., Brownell, L.E., 1954. Residual equilibrium saturation of porous media. Ind. Eng. Chem. 46, 1207–1219.

Greig, C., 1995. Studies on Continuous Sugar Centrifuges. Ph.D. Thesis, Department of Chemical Engineering, University of Queensland.

Greig, C., Kelly, J., White, E., Kirby, L., 1984. Corrosion and erosion of fugal screens. In: Proceedings of Australian Society of Sugar Cane Technologists.

Grimwood, C., 2007. Course Notes for Centrifugation. Raw Cane Sugar Manufacturers' Institute, Nicholls State University, Louisiana.

Grimwood, G.C., Thewlis, M.J., Dean, A.J., 2005. Efficient centrifugal operation. Int. Sugar J. 107 (1284) 680, 682–684, 686–687.

Leung, W.W.F., 1998. Industrial Centrifugation Technology. McGraw-Hill, New York.

Makarytchev, S.V., Langrish, T.A.G., Prince, R.G.H., 1998. Structure and regimes of liquid film flow in spinning cone columns. Chem. Eng. Sci. 53, 1541–1550.

Makarytchev, S.V., Xue, E., Langrish, T.A.G., Prince, R.G.H., 1997. On modelling fluid flow over a rotating conical surface. Chem. Eng. Sci. 52, 1055–1057.

Nielsen, P., 1992. Coastal Bottom Boundary Layers and Sediment Transport. Advanced Series on Ocean Engineering. World Scientific, Singapore, River Edge, NJ.

Nigmatulin, R.I., 1991. Dynamics of Multiphase Media, rev. and augm. edition. Hemisphere Pub. Corp., New York.

Norem, H., Locat, J., Schieldrop, B., 1990. An approach to the physics and the modeling of submarine flowslides. Mar. Geotechnol. 9, 93–111.

Oliver, D.R., Ward, S.G., 1953. Relationship between relative viscosity and volume concentration of stable suspensions of spherical particles. Nature 171, 396–397.

Raudkivi, A.J., 1967. Loose Boundary Hydraulics. Pergamon Press.

Rouillard, E., Koenig, M., 1980. The viscosity of molasses and massecuite. In: Proceedings of The South African Sugar Technologists' Association, pp. 89–92.

Soltani, F., Yilmazer, U., 1998. Slip velocity and slip layer thickness in flow of concentrated suspensions. J. Appl. Polym. Sci. 70, 515–522.

Swindells, R., 1982. A mathematical model of a continuous sugar centrifuge. Ph.D. Thesis, Department of Chemical Engineering, University of Queensland.

Symons, D.D. Frictional flow of damp granular material in a conical centrifuge. Journal of Mechanical Engineering Science, in press. doi:10.1177/0954406211412466.

Symons, D.D., 2011b. Integral methods for flow in a conical centrifuge. Chem. Eng. Sci. 66, 3020–3029.

Tarleton, E.S., Wakeman, R.J., 2007. Solid/liquid Separation: Equipment Selection and Process Design. IChemE Series. Butterworth-Heinemann.

Terzaghi, K., 1960. From Theory to Practice in Soil Mechanics; Selections from the Writings of Karl Terzaghi, with Bibliography and Contributions on his Life and Achievements. Wiley, New York.

Wakeman, R., 1977. Dewatering properties of particulate beds. J. Powder Bulk Solids Technol. 1, 64–69.

White, N., Duke, H., Sunada, D., Corey, A., 1970. Physics of desaturation in porous materials. J. Irr. Div. Am. Soc. Civ. Eng. Proc. 96, 165–191.

Wolfram Research, I., 2008. Mathematica 7.01.0.

Yilmazer, U., Kalyon, D.M., 1989. Slip effects in capillary and parallel disk torsional flows of highly filled suspensions. J. Rheol. 33, 1197–1212.